separations

MDPI

Article

Green Synthesis of Thiourea-Grafted Activated Carbon for Efficient Adsorption of $AuCl_4^-$

Tianyi Chen [1,2], Xudong Liu [1,2,*], Yaobin Lai [1,2,3,*], Jiayi Zan [1,2] and Xuxia Zhang [1,2,3,*]

[1] School of Rare Earth, University of Science and Technology of China, Hefei 230026, China; tychen23@gia.cas.cn (T.C.); jyzan23@gia.cas.cn (J.Z.)
[2] Ganjiang Innovation Institute of the Chinese Academy of Sciences, Ganzhou 341000, China
[3] Jiangxi Province Key Laboratory of Cleaner Production of Rare Earths, Ganzhou 341000, China
* Correspondence: xdliu@gia.cas.cn (X.L.); yblai@gia.cas.cn (Y.L.); xxzhang@gia.cas.cn (X.Z.)

Abstract

The thiourea grafting method can effectively improve the ability of activated carbon to recover chloroauric acid ($AuCl_4^-$). Conventional grafting strategies rely on acyl halide reactions using reagents such as $SOCl_2$ and CH_2Cl_2, which suffer from instability and high toxicity. Herein, we propose a green grafting strategy for thiourea by activating carboxyl groups with EDC-HCl/NHS in acetonitrile, followed by the amidation reaction to obtain thiourea-modified carbon (AC-NCS). FT-IR and XPS analyses confirm the successful grafting of thiourea onto the activated carbon surface. Compared with pristine activated carbon, the adsorption capacity of AC-NCS is 104.8 mg/g, increased by 5.76 times. Furthermore, it maintains a recovery rate of 84.2% after three cycles. XPS and FT-IR further reveal that adsorption occurs on the thiourea sulfur atoms (C=S) and protonated primary amines(-NH_3^+), and the recovery of chloroauric acid is achieved through a synergistic "reduction–electrostatic attraction" mechanism. This method reduces the dependence on highly toxic reagents and provides a promising approach for the efficient and green recovery of gold from secondary resources.

Keywords: efficient gold recovery; amidation; thiourea; green synthesis

1. Introduction

Gold is a precious metal known for its outstanding physicochemical properties. Its electrical conductivity and thermal conductivity are 41.0 × 10^6 S/m and 318 W/(m·K), respectively, second only to those of silver and copper. Gold is relatively soft, resistant to oxidation and acid corrosion, and excessive mining has imposed severe pressure on the ecological environment. These characteristics render gold widely applicable in numerous fields [1]. However, the difficulty and cost of gold mining have been increasing annually, and excessive mining imposes significant pressure on the ecological environment [2]. At the same time, the loss of gold during its subsequent production and application cannot be ignored—this process is often accompanied by the discharge of large volumes of gold-containing wastewater. If left untreated, this directly results in the loss of gold resources [3]. Recently, recycling valuable resources from wastewater has gained increasing attention. The approaches highlight the potential of waste-to-resource strategies [4]. Therefore, the efficient recovery of gold from wastewater is not only a necessary measure to reduce resource waste but also helps to lower the demand for primary gold mining.

Currently, the methods for recovering gold from wastewater mainly include solvent extraction [5], membrane separation [6,7], reduction [8], and adsorption [9]. Among them,

Academic Editor: Che-Jung Hsu

Received: 12 May 2026
Revised: 2 June 2026
Accepted: 8 June 2026
Published: 17 June 2026

adsorption is particularly suitable for gold-containing wastewater with complex compositions and low gold concentrations, and is thus the most widely applied [10,11]. For example, Ren et al. designed a magnetically driven MXene/Graphene oxide hydrogel, which enables highly selective gold recovery from strong acidic wastewater. Through a "magnetic-adsorption-reduction" synergistic mechanism, the adsorption capacity is 2821.8 mg/g and gold purity of 99.9%, demonstrating that integrating adsorption and reduction functions into a single material is a promising strategy for efficient gold recovery [12].

As the most widely used material in adsorption methods, activated carbon offers several advantages, including low cost, high stability, and a large specific surface area. It has been widely applied in the recovery of gold from cyanide leaching tailings [13–15]. It has been demonstrated that the adoption of different activation strategies can potentially enhance the adsorption capacity of activated carbon toward specific molecules [16]. However, activated carbon has limited inherent active sites and its surface carries negatively charged oxygen-containing groups, which electrostatically repel the similarly negatively charged, bulky gold–chloro complex anions, thereby impeding their adsorption and recovery. In view of the strong coordination ability of thiourea toward gold ions, functionalizing activated carbon with thiourea offers a feasible solution to this problem [17].

According to different modification routes, the strategies for enhancing gold adsorption performance using thiourea can be classified into three categories: (1) Physical mixing -impregnation: thiourea is loaded onto AC via hydrogen bonding or physical adsorption, requiring only mixing, impregnation, and drying. Although simple to operate, the loaded thiourea is prone to detachment and loss under mechanical agitation, significantly reducing the adsorption lifetime [18]. (2) High-temperature pyrolysis: thiourea and AC are co-pyrolyzed under a protective atmosphere, and the nitrogen and sulfur atoms derived from thiourea decomposition are incorporated into the carbon lattice, forming N,S-doped carbon. The mechanism of gold recovery by this material is fundamentally different from that of thiourea [19]. (3) Chemical grafting method: Thiourea molecules are anchored onto the AC surface via covalent bonds, improving its adsorption selectivity. The electrophilicity of the carboxyl groups on the activated carbon surface is relatively weak, resulting in low grafting efficiency. In the laboratory, acyl halide reactions are commonly employed to activate the carboxyl groups on activated carbon to promote grafting [20,21]. However, this system involves reagents such as thionyl chloride and dichloromethane, its instability and high toxicity are inconsistent with the concept of green synthesis.

In light of this, the present study reports a more environmentally friendly and efficient method for the grafting of thiourea onto activated carbon. By employing N-Hydroxysuccinimide/1-Tthyl-3-(3-dimethylaminopropyl) carbodiimide hydrochloride coupling reagents, a relatively stable activated carboxyl intermediate was obtained, and the thiourea-grafted modified carbon, designated as AC-NCS, was successfully prepared. Based on this, the recovery behavior and adsorption mechanism of this material toward chloroauric acid were further investigated.

2. Characterization and Preparation

2.1. Characterization

Fourier transform infrared (FTIR) spectra were recorded on a Nicolet iS5 spectrometer (Thermo Fisher Scientific Inc., Waltham, MA, USA) to analyze the surface functional groups of the samples. Prior to measurement, a background spectrum was collected using thoroughly dried KBr (purity 99%) as the reference. The dried sample was then mixed with KBr at a mass ratio of 1:100 and ground to a fine powder. The mixture was pressed into a transparent pellet for analysis. The spectra were acquired in the wavenumber range of 4000–400 cm^{-1} with a resolution of 4 cm^{-1}, and 16 scans were co-added per spectrum.

X-ray photoelectron spectroscopy (XPS) was performed on an AXIS SUPRA+ X-ray photoelectron spectrometer (Shimadzu Corporation, Kyoto, Japan) using monochromatic Al Kα radiation (hν = 1486.6 eV) operated at 150 W, and the pass energy for high-resolution spectra was set to 50 eV. All binding energies were calibrated with reference to the C 1s peak at 284.8 eV.

The structure of the powder samples was characterized using an InVia confocal Raman spectrometer (Renishaw plc, Wotton-under-Edge, UK). The powder samples were evenly spread onto a concave quartz glass slide and focused using a 50× objective lens. The laser wavelength was 532 nm, and the grating was 1800 lines/mm.

The morphology and surface elemental composition of the samples were characterized using a JSM-IT800 scanning electron microscope (SEM) (JEOL Ltd., Akishima, Japan). The specific surface area and pore structure of the samples were analyzed by nitrogen adsorption–desorption measurements using an ASAP 2460 surface area and porosity analyzer (Micromeritics Instrument, Norcross, GA, USA). Prior to the measurement, the sample was degassed at 160 °C for 2 h to remove physically adsorbed water and gases. Nitrogen adsorption–desorption isotherms were measured at liquid nitrogen temperature (77 K).

The concentration of metal ions in the solution samples was determined using a PQ9000 inductively coupled plasma optical emission spectrometer (ICP-OES) (Analytik Jena AG, Jena, Germany). The calibration curve was constructed using standard solutions with a series of concentration gradients, which were prepared by diluting national standard samples. Prior to measurement, all samples were filtered through a 0.22 μm polytetrafluoroethylene (PTFE) membrane filter. Calibration curves were constructed based on these standard solutions, and the correlation coefficient (R^2) was required to be no less than 0.999. The concentration of each test sample fell within the range of the calibration curves.

2.2. Preparation of Thiourea-Grafted Modified Carbon (AC-NCS)

Commercial activated carbon was first oxidized according to the method reported by Figueiredo [22]. All reagents used for the synthesis in this work are listed in Table S1. Typically, 200 mg of commercial activated carbon was mixed with 100 mL of 6 mol/L H_2SO_4 solution at 60 °C for 4 h. The resulting solid was washed with deionized water until the washing solution reached a neutral pH, and then dried in an oven at 80 °C for 24 h to obtain the oxidized activated carbon. Subsequently, 100 mg of the oxidized activated carbon and 17.3 mg of NHS were placed in 50 mL of acetonitrile and mixed at 60 °C under stirring at 300 r/min for 10 min to ensure sufficient penetration of NHS into the pores of the activated carbon. Then, 47.9 mg of EDC-HCl was quickly added, and the reaction was allowed to proceed at 60 °C under stirring at 300 r/min for 3 h. After the reaction, the mixture was vacuum-filtered, and the solid was washed three times with acetonitrile to remove the reaction intermediates, yielding the modified carbon with grafted activated carboxyl groups. Thereafter, 76 mg of thiourea and 2.4 mg of 4-dimethylaminopyridine (DMAP), used as an acylation catalyst, were rapidly mixed with the above modified carbon in 50 mL of acetonitrile. The reaction mixture was maintained at 60 °C in a water bath for 12 h. The preparation process is shown in Figure 1. Upon completion, the activated carbon was collected, washed repeatedly with ethanol and water, and finally dried at 60 °C for 6 h to obtain the thiourea-grafted modified carbon, designated as AC-NCS.

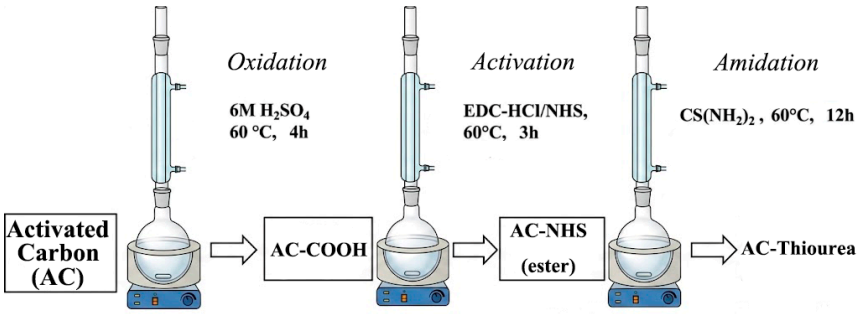

Figure 1. Schematic illustration of the grafting reaction.

3. Results

3.1. Structural Characterization of Thiourea-Grafted Activated Carbon

3.1.1. Raman Spectroscopic Characterization and Analysis

Raman spectroscopy was employed to detect the structural changes in activated carbon before and after thiourea grafting, and the results are shown in Figure 2. The D band and G band of carbon appear at 1355 cm^{-1} and 1591 cm^{-1}, respectively, corresponding to the degree of atomic disorder in the carbon layer structure and the graphitization crystallinity [23].

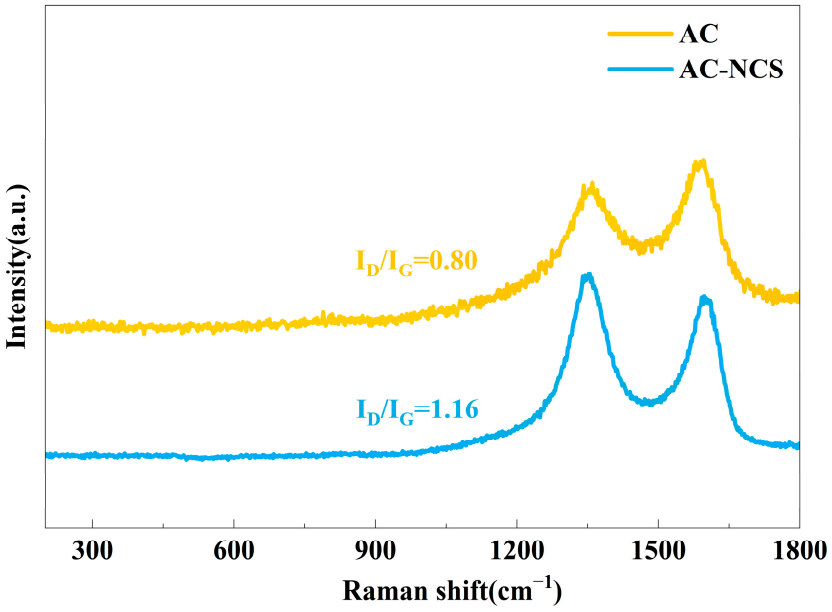

Figure 2. Raman spectra of activated carbon before and after thiourea grafting.

As shown in Figure 2, after thiourea modification, the I_D/I_G ratio increased from 0.80 to 1.16, indicating an increase in the disorder degree of activated carbon. Prior to thiourea grafting, the activated carbon was subjected to sulfuric acid etching to introduce sufficient carboxyl groups, providing abundant active sites for subsequent covalent grafting of thiourea. During the oxidation process, the well-ordered graphitic carbon structure on the activated carbon surface was oxidized, generating a substantial amount of amorphous carbon bearing oxygen-containing functional groups, which disrupted the integrity of the lattice atomic arrangement. Meanwhile, the oxidizing environment of hot acid etching caused certain corrosion to the carbon skeleton, readily inducing structural defects such as pore wall collapse and crystal wrinkles, further increasing the structural disorder of the carbon material from a physical structure perspective. Overall, the Raman spectroscopic characterization results indicate that the two-step process of sulfuric acid oxidation pretreat-

ment followed by covalent thiourea grafting collectively enhances the structural disorder of activated carbon and provides more active sites for the grafting of thiourea molecules.

3.1.2. Study on Surface Morphology and Pore Structure

The morphology and microstructure of AC-NCS were measured: As shown in Figure 3a, SEM images showed a smooth surface morphology, and EDS mapping revealed that the distribution of O, S, and N elements closely followed that of the carbon matrix (Figure 3b–d). The mass ratio of O:N:S was determined to be approximately 6.7:3.2:1 by EDS quantification. This low sulfur content implies that the free hydroxyl groups on the acid-etched carbon surface are not efficient anchoring sites for thiourea grafting. BET analysis (Figure 3e,f) demonstrated that the specific surface area increased from 583 to 841 m^2/g after modification, suggesting that acid etching generated additional pore channels—a conclusion supported by the increased amorphous carbon ratio observed in Raman spectra. Overall, the acid etching and subsequent thiourea functionalization produce an activated carbon with an enlarged specific surface area and abundant N- and S-active sites, both of which are favorable for the adsorption of chloroaurate ions.

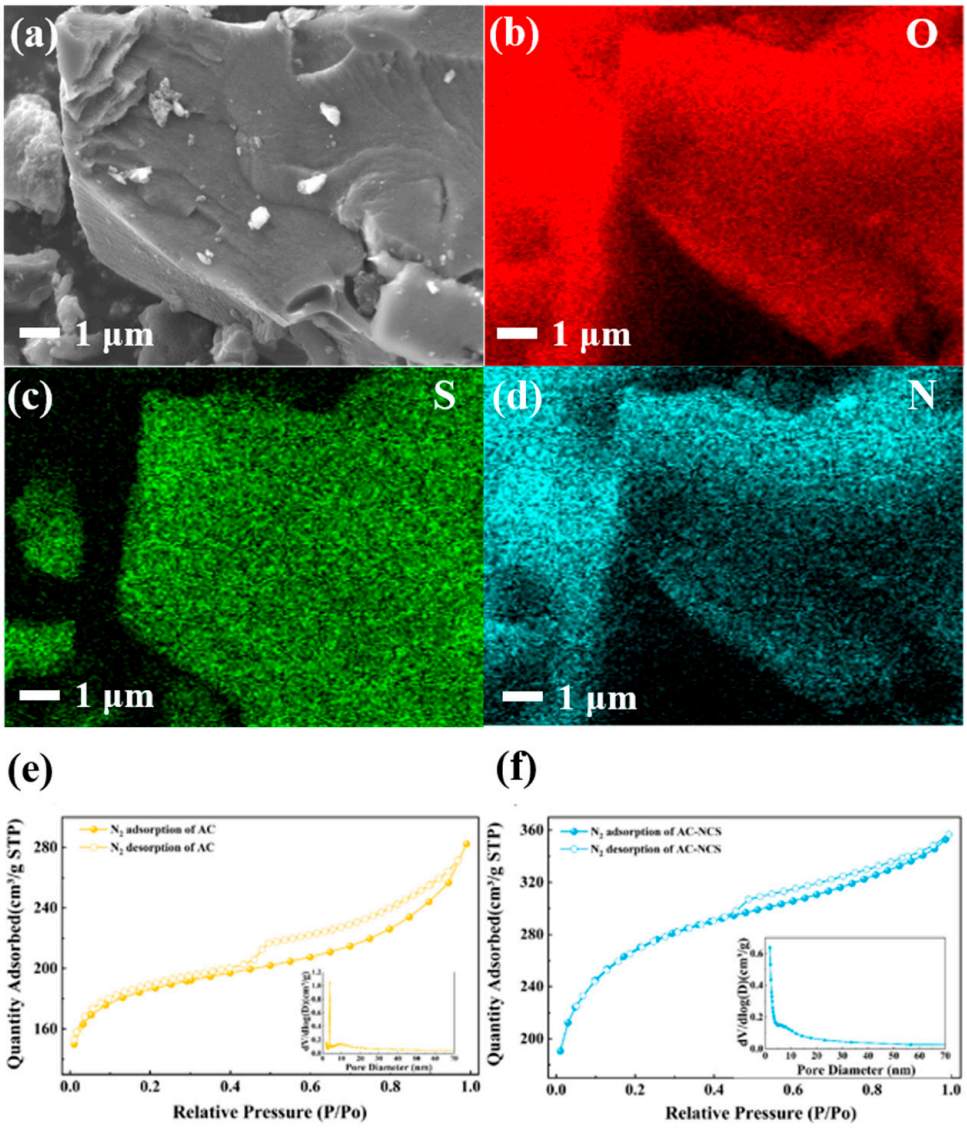

Figure 3. (**a**–**d**) SEM image of AC-NCS and distribution of O, S and N, (**e**,**f**) BET isotherm of AC (before grafting) and AC-NCS (Yellow curve for AC and blue curve for AC-NCS).

3.1.3. FT-IR Spectroscopic Characterization and Analysis

To verify the successful occurrence of the amidation reaction and thiourea grafting, FT-IR spectra of the activated carbon samples before and after the reaction, as well as of AC-NCS, were recorded, and the results are shown in Figure 4. Before modification, only a small amount of bound water was present on the activated carbon surface. The absorption peaks at 1380 cm^{-1}, 1132 cm^{-1}, and 1085 cm^{-1} are attributed to the vibration modes of the conjugated aromatic ring, saturated C–H bonds, and the mixed carbon chain skeleton, respectively [24].

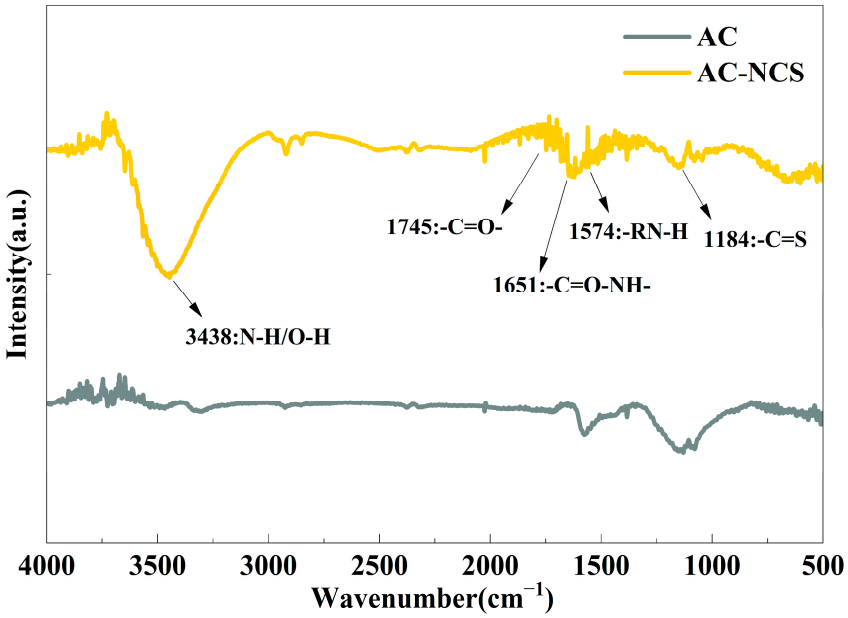

Figure 4. FT-IR spectra of activated carbon before and after grafting.

After the grafting reaction, a set of medium-intensity absorption peaks with similar intensity and relatively broad shapes appeared in the range of 1386–1692 cm^{-1}. Among them, the peak at 1651 cm^{-1} corresponds to the stretching vibration of the amide C=O group, while the peaks at 3438 cm^{-1} and 1574 cm^{-1} are assigned to the stretching and bending vibration modes of N–H, respectively [25,26]. The peak at 1184 cm^{-1} is attributed to the C=S stretching vibration, whose wavenumber is relatively low due to the electron-donating conjugation effect [27]. These spectral changes indicate that the amidation reaction proceeded successfully and that the oxidized activated carbon was converted into the thiourea-grafted modified carbon AC-NCS. Additionally, the weakest signal at 1745 cm^{-1} suggests that the number of carboxyl grafting sites introduced onto the activated carbon surface by strong acid oxidation remains limited.

3.1.4. XPS Surface Elemental Characterization and Analysis

To further confirm whether thiourea was covalently loaded onto the activated carbon surface, X-ray photoelectron spectroscopy (XPS) analysis was performed. The survey spectrum (Figure 5) shows that the sample surface is primarily composed of C and O elements, along with characteristic S 2p and N 1s signals appearing near 162–170 eV and 398–410 eV, respectively.

The unmodified carbon was characterized using XPS. The survey spectrum showed almost no N or S signals (Figure 5a), and the high-resolution C 1s spectrum indicated only a few oxygen-containing functional groups on the surface (Figure 5b). The high-resolution C 1s spectrum of AC-NCS was deconvoluted (Figure 5d), with fitted peaks at 284.8 eV, 285.9 eV, 287.2 eV, and 288.5 eV corresponding to the backbone sp^2 and sp^3 hybridized

carbon atoms, C–NH carbon atoms in the grafted structure, the C=S carbon of the amide group, and the surface C–O/C=O oxidized carbon, respectively.

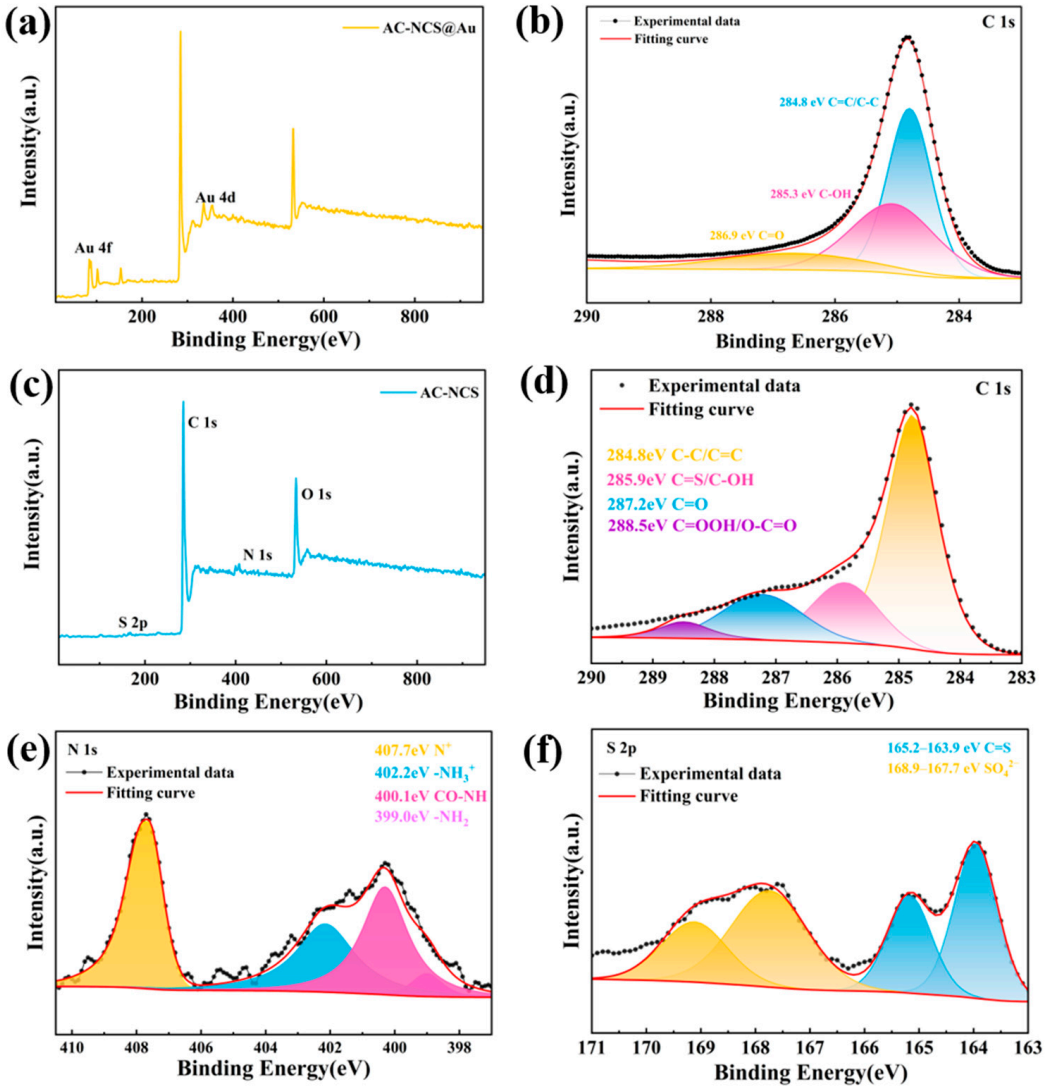

Figure 5. (**a**) XPS survey spectrum of active carbon (AC), (**b**) high-resolution C 1s spectrum of AC, (**c**) XPS survey spectrum of AC-NCS, (**d**) high-resolution C 1s, (**e**) N 1s, and (**f**) S 2p spectrum.

Analysis of the high-resolution N 1s spectrum (Figure 5e) reveals that the peak at 407.67 eV corresponds to high-valence nitrogen atoms originating from residual quaternary ammonium intermediates, which play no role in gold recovery. Excluding the high-valence nitrogen, the fitted peak at 398.98 eV shows the largest area, accounting for 51.64%, and is attributed to $–NH_2$ groups not involved in the grafting reaction. The peak at 400.10 eV corresponds to the nitrogen atom of the amide bond, accounting for 41.93%. A small fraction of nitrogen species with a higher binding energy (402.18 eV) is observed, which is speculated to arise from weak hydrogen bonding between surface hydroxyl groups and $–NH_2$, or from resonance between aromatic carbon and grafted nitrogen atoms, as also reported in the literature [28–30].The high-resolution S 2p spectrum (Figure 5f) can be deconvoluted into four peaks. The peaks at 163.93 eV and 165.17 eV correspond to the sulfur atoms of thiourea, while the peaks at 167.74 eV and 168.92 eV are attributable to unreacted NHS and its active esters, as well as residual oxidized SO_4^{2-} species [31]. The appearance of these signals confirms that thiourea molecules are chemically linked to the activated carbon surface via amide bonds, thereby improving the grafting stability.

Combining the FT-IR and XPS results, it is confirmed that thiourea has been successfully grafted onto the activated carbon surface through the amidation reaction.

3.2. Adsorption Behavior Study

To investigate the adsorption behavior and mechanism of chloroaurate ions on the modified activated carbon, the effect of enhanced mass transfer under different stirring rates on the adsorption performance was first examined. On this basis, the adsorption capacity, adsorption isotherms, and adsorption thermodynamics of the modified activated carbon were studied.

3.2.1. Effect of Stirring Speed on Adsorption Kinetics

A 100 mL aliquot of low-concentration chloroauric acid solution (measured concentration: 15 ± 0.5 mg/L) was prepared, and 10 mg of modified activated carbon was added. The mixture was stirred at room temperature at speeds of 0, 100, 200, and 300 r/min, respectively. The concentration of $AuCl_4^-$ in the solution was monitored at different time intervals.

As shown in Figure 6, two minutes after the addition of the adsorbent, the concentration of $AuCl_4^-$ decreased by 0.66, 3.36, 3.97, and 4.3 mg/L at stirring speeds of 0, 100, 200, and 300 r/min, respectively. Visual observation during the initial stage of adsorption revealed that at a stirring speed of 0 r/min, the activated carbon tended to aggregate and float on the liquid surface due to its low density and insufficient surface wetting, which limited effective contact with $AuCl_4^-$. Upon the introduction of stirring, as the rotational speed increased, the fluid shear force gradually dispersed the activated carbon particles, significantly enhancing the solid–liquid contact efficiency and facilitating rapid migration of $AuCl_4^-$ toward the adsorbent surface. At stirring speeds of 100, 200, and 300 r/min, the half-life of the $AuCl_4^-$ concentration was shortened from approximately 120 min to 30 min. Under static adsorption conditions (0 r/min), although a certain adsorption capacity was observed within 120 min, the actual adsorption capacity fluctuated. This phenomenon is speculated to arise from the weak interaction between the primary amine groups and gold ions, indicating that the system had not yet reached adsorption equilibrium. In this case, $AuCl_4^-$ had not been reduced to the elemental state and was only transiently captured at the solid–liquid interface. When the stirring speed was increased to 300 r/min, adsorption reached equilibrium within 120 min, suggesting that this stirring speed is more favorable for the adsorption of low-concentration gold solutions. Therefore, a stirring speed of 300 r/min was selected for subsequent experiments.

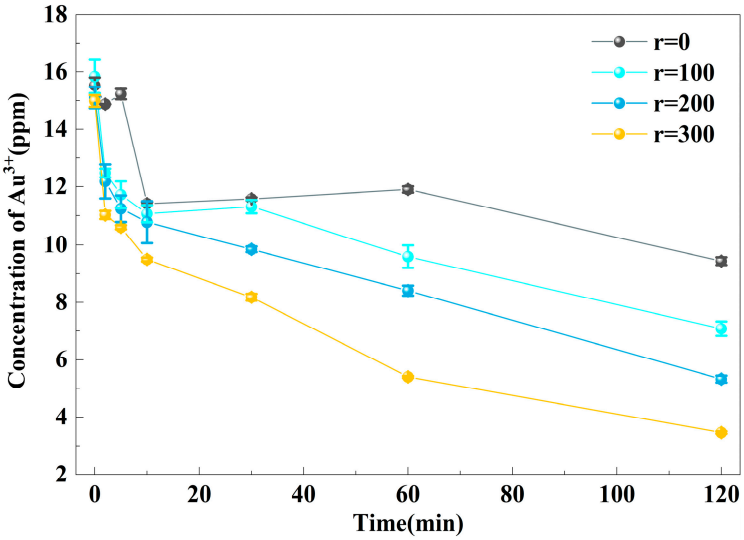

Figure 6. Effect of stirring speed on the adsorption of chloroauric acid.

3.2.2. Adsorption Isotherm Study

To investigate the adsorption performance of the obtained modified carbon toward gold, the adsorption capacity was measured at different initial concentrations. Chloroauric acid solutions (50 mL, pH = 1) with initial concentrations of 4, 8, 16, 32, and 50 mg/L (error ± 0.5 mg/L) were prepared. The mass of adsorbent used was 10 mg (error ± 0.2 mg).

The fitting results are shown in Figure 7. The correlation coefficient (R^2) obtained from the Langmuir model was 0.9226, and the fitted maximum adsorption capacity was 109.54 mg/g, which was closest to the experimentally measured adsorption capacities (104.18 and 104.76 mg/g at initial concentrations of 32 and 50 mg/L, respectively). In contrast, the correlation coefficient for the Freundlich model was only 0.6601 (Table 1). These results indicate that (1) the adsorption is dominated by monolayer adsorption. Thiourea is grafted onto the activated carbon surface rather than into pores or collapsed multilayer topological regions, and the homogeneous surface serves as the main site for adsorption. (2) In the Freundlich model, n = 5.02, suggesting that the chemisorption of gold through the interaction between the sulfur atoms of thiourea and Au proceeds as expected. The relatively low correlation coefficient indicates that other mechanisms are involved in the gold recovery process besides chemical reduction. This is attributed to the fact that some primary amine groups do not participate in the amidation reaction and, upon protonation, undergo electrostatic interactions with the negatively charged chloroaurate ions [17], leading to the fitting models not fully describing the adsorption process.

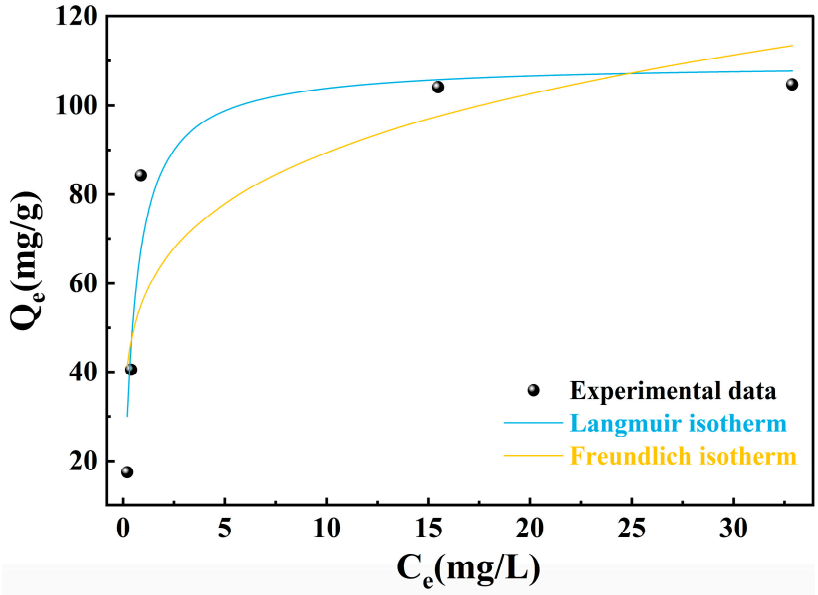

Figure 7. Adsorption isotherms of AC-NCS and fitting curves by Langmuir and Freundlich models.

Table 1. Parameters of Langmuir and Freundlich isotherm models for AC-NCS.

Langmuir Adsorption Isotherm			Freundlich Adsorption Isotherm		
q_e (mg/g)	K_L (L/mg)	R_L^2	n	K_F ((mg/g)(L/mg))$^{1/n}$	R_F^2
109.54	1.84	0.9226	5.02	56.54	0.6601

3.2.3. Adsorption Thermodynamics Study

The effect of temperature on the adsorption rate and kinetics was investigated: 50 mL of low-concentration $AuCl_4^-$ solution was prepared, and 10 mg of AC-NCS was added. The concentration of $AuCl_4^-$ in the solution was measured at regular intervals at 293 K,

313 K, 333 K, and 353 K, and the corresponding adsorption capacities were calculated. The results are shown in Figure 8a,b.

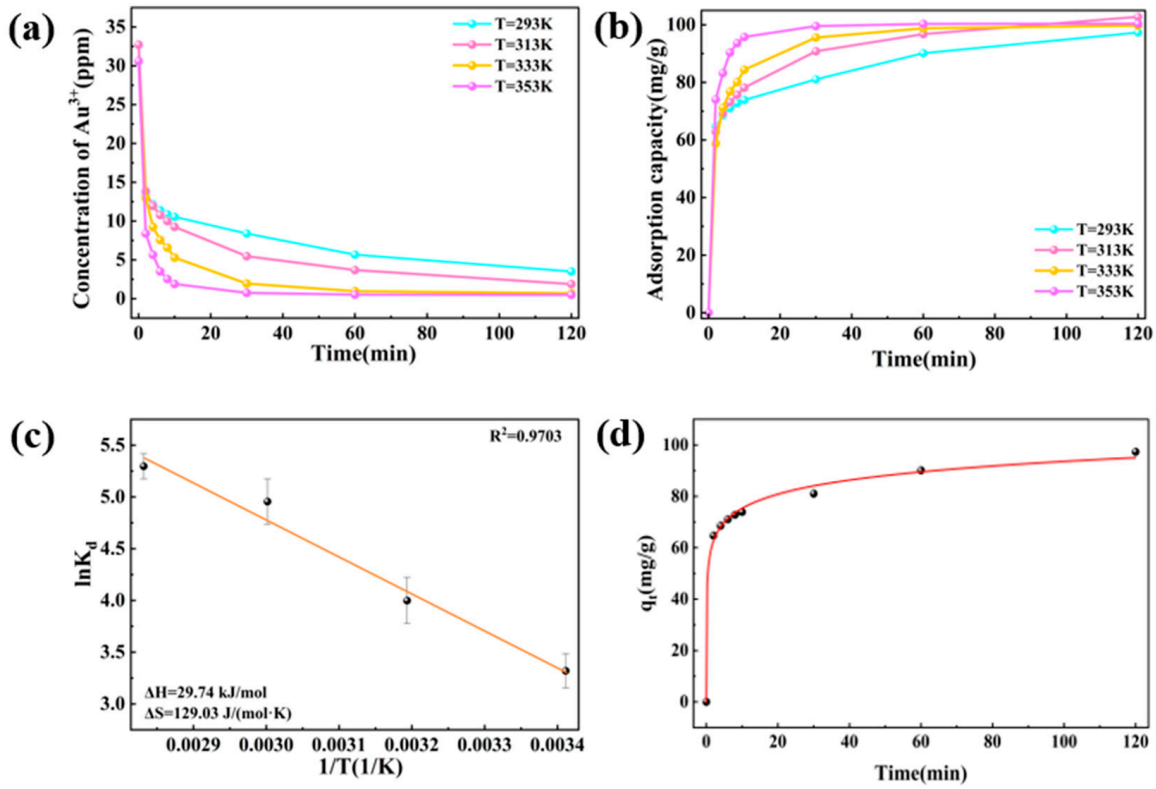

Figure 8. (**a**) Time-dependent concentration of $AuCl_4^-$ at different temperatures, (**b**) adsorption capacity at different temperatures, (**c**) Van't Hoff plot for thermodynamic parameters, (**d**) Elovich model fitting plot for the adsorption of gold ions.

Under enhanced mass transfer conditions, the concentration of chloroauric acid decreased rapidly and nearly reached equilibrium within 2 h. The equilibrium concentrations were 3.52, 1.88, 0.70, and 0.50 mg/L, respectively. By calculating the adsorption thermodynamics (Figure 8c), the enthalpy change (ΔH) before and after adsorption was determined to be 29.74 kJ/mol, indicating that the adsorption process is endothermic, and increasing the temperature favors the forward adsorption reaction. Furthermore, the entropy change (ΔS) of the reaction was 129.03 J/(mol·K), suggesting the dissociation of chloroaurate ions into gold atoms and chloride ions during the adsorption process [22]. According to the fitted equation, the Gibbs free energy at room temperature (25 °C) was calculated to be −8.08 kJ/mol, confirming that the reaction proceeds spontaneously at ambient temperature. However, the increase in temperature resulted in only a limited enhancement of the adsorption capacity, with a slightly better effect on the adsorption rate. Considering the susceptibility of thiourea to decomposition and the oxidative environment on the activated carbon surface, excessively high adsorption temperatures should be avoided. To further elucidate the adsorption kinetics under the enhanced mass transfer conditions, the experimental data under 20 °C were fitted with the Elovich kinetic model. As shown in Figure 8d and Table 2), the Elovich model yielded an excellent correlation coefficient (R^2 = 0.996) for the adsorption of chloroauric acid onto AC-NCS. This good fit suggests that the adsorption of gold species involves a chemisorption mechanism with an energetically heterogeneous surface, which is consistent with the presence of thiourea functional groups acting as active sites.

Table 2. Kinetic parameters of the Elovich model for AC-NCS.

Elovich Model		
A (mg/(g·min))	B (g/mg)	R_e^2
10,761.23	0.126	0.99644

3.2.4. Adsorption Kinetics Study

The linear fitting results of the pseudo-second-order model are shown in Figure 9. The pseudo-first-order model gave relatively high correlation coefficients at lower temperatures (293 K and 313 K), with R^2 values of 0.8876 and 0.9078, respectively. However, when the temperature was raised to 333 K and 353 K, the pseudo-first-order model could only reasonably describe the adsorption behavior within the first 30 min and 10 min of adsorption, respectively, with linear correlation coefficients of 0.9523 and 0.9927 (Figure S1). This is consistent with the conclusion that increasing temperature promotes the reductive recovery of $AuCl_4^-$. As the concentration of surface active sites continues to decrease, the adsorption kinetics become severely limited, and the reduction no longer occurs only on the surface but extends into the deep pores, exhibiting adsorption behavior influenced by diffusion kinetics.

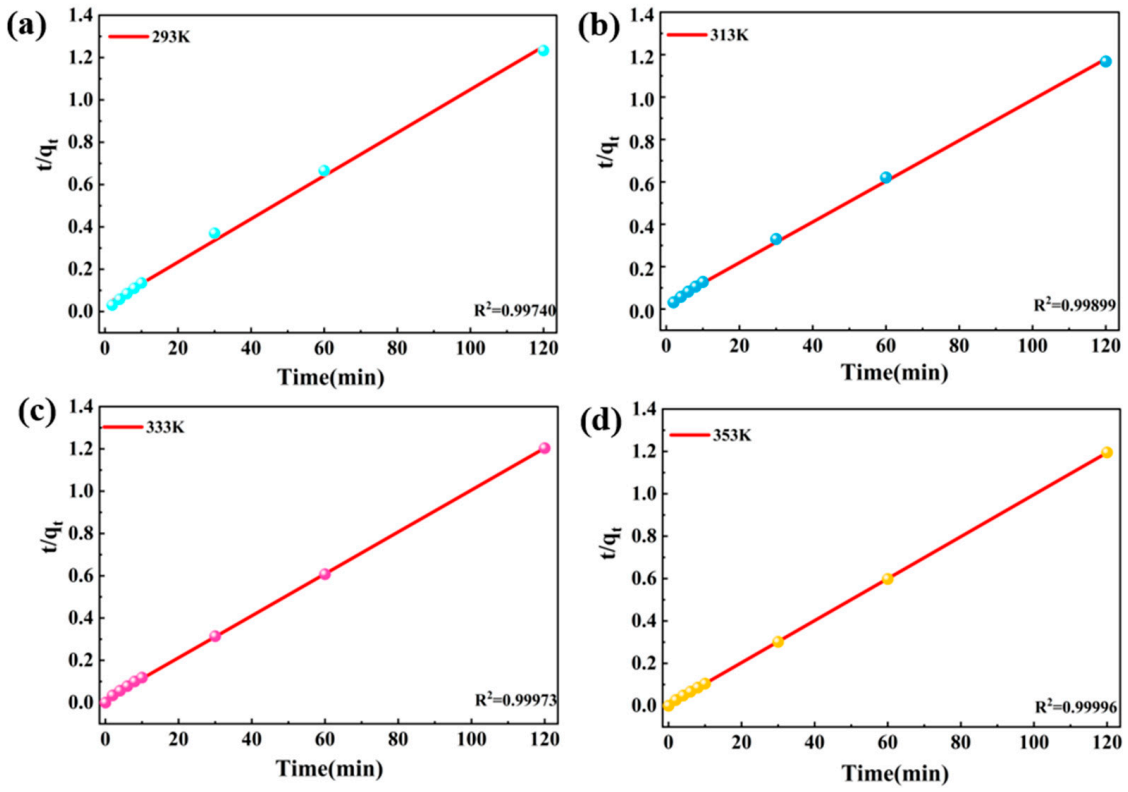

Figure 9. Pseudo-second-order kinetic linear plots for gold adsorption at (**a**) 293 K, (**b**) 313 K, (**c**) 333 K, and (**d**) 353 K.

The correlation coefficients for the pseudo-second-order model fittings were all above 0.99, confirming that chemisorption dominates the adsorption process. As the temperature increased, the pseudo-second-order rate constant decreased from 0.0101 to 0.0099, which is attributed to the instability of the grafted thiourea molecules at elevated temperatures. The adsorption capacity was only marginally affected by temperature within 2 h; when the thiourea grafting density was similar, the dispersibility and mass transfer capability of the adsorbent itself became the determining factors.

3.2.5. Adsorption Selectivity Study

Adsorbents often suffer from insufficient selectivity because active sites bind to other metal ions, resulting in inadequate $AuCl_4^-$ recovery. Therefore, the selective recovery capacity of the modified carbon toward $AuCl_4^-$ was investigated. A simulated real solution containing 5 ± 0.5 mg/L gold ions and 100 ± 15 mg/L metal impurity ions (pH = 1) was prepared at an atomic mass ratio of 1:20. The results are shown in Figure 10:

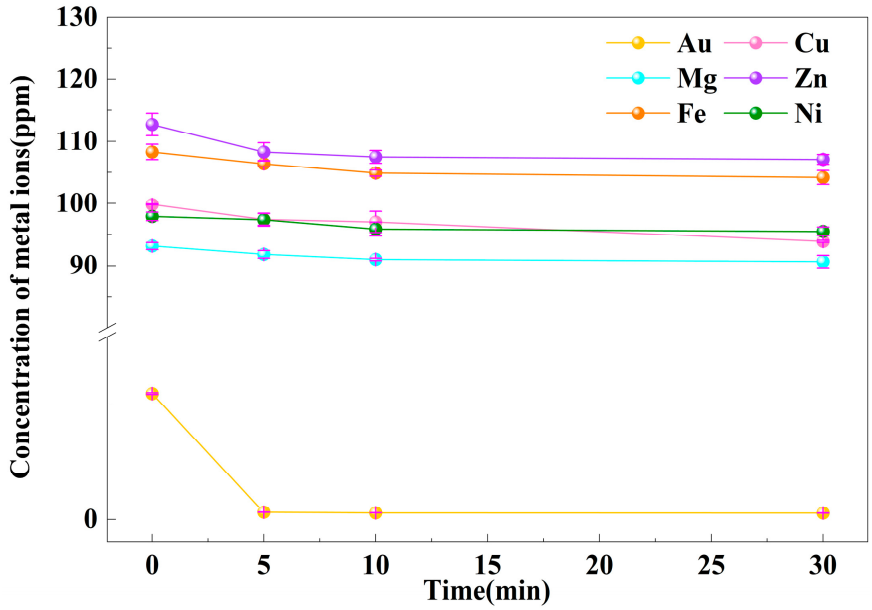

Figure 10. Adsorption selectivity experiment.

Due to the low concentration of $AuCl_4^-$, its concentration decreased from 5.50 mg/L to 0.31 mg/L within 5 min and remained essentially stable over the next half-hour (with a concentration fluctuation of only 0.3 mg/L within 30 min). Within the first 5 min, the concentrations of Mg^{2+}, Fe^{3+}, Cu^{2+}, and Ni^{2+} decreased by less than 2 mg/L, while Zn^{2+} exhibited the largest decrease of 4.4 mg/L. The adsorption capacities of the modified carbon toward gold and the other metal ions at 5 min and 30 min were calculated, and the results are shown in Table 3.

Table 3. Adsorption capacity of modified carbon for various metal ions at 5 min and 30 min.

	Au (mg/g)	Cu (mg/g)	Mg (mg/g)	Zn (mg/g)	Fe (mg/g)	Ni (mg/g)
5 min	51.9	24.1	13.3	40.4	19.0	5.3
30 min	52.3	39.9	24.9	51.6	41.1	24.0

As shown in Table 3, the competition between Zn^{2+} and $AuCl_4^-$ was pronounced within the first 5 min. This is because Zn^{2+} is a borderline acid belonging to the soft acid category, which has a certain affinity for the soft base sulfur atoms, thereby competing with gold for active sites [32]. Considering that the concentration of Zn^{2+} was much higher than that of $AuCl_4^-$, AC-NCS still exhibited good selectivity. Furthermore, under acidic conditions, iron ions catalyze the oxidative decomposition of thiourea functional groups, generating formamidine disulfide and even elemental sulfur. This accounts for the significant decrease in Fe^{3+} concentration observed after 30 min.

3.2.6. Cyclic Adsorption Performance Study

The cyclic performance of the modified carbon was investigated through repeated adsorption–desorption experiments to evaluate its practical application potential. The specific experimental procedure was as follows: 100 mL of a 20 mg/L chloroauric acid solution was prepared, and 10 mg of the thiourea-modified carbon was added. The adsorption was carried out for 1 h, after which the concentration of $AuCl_4^-$ in the supernatant was measured. For desorption, 50 mL of an eluent consisting of 0.1 M thiourea, 0.1 M H_2SO_4, and 0.25 M iron ions was prepared. The modified carbon loaded with gold was ultrasonically eluted for 30 min. After desorption, the modified carbon was separated, washed, and dried at 60 °C. It was then directly used for the second adsorption cycle under identical conditions. This procedure was repeated four times. The recovery rate was calculated based on the residual $AuCl_4^-$ concentration in the solution after each cycle. The results are shown in Figure 11.

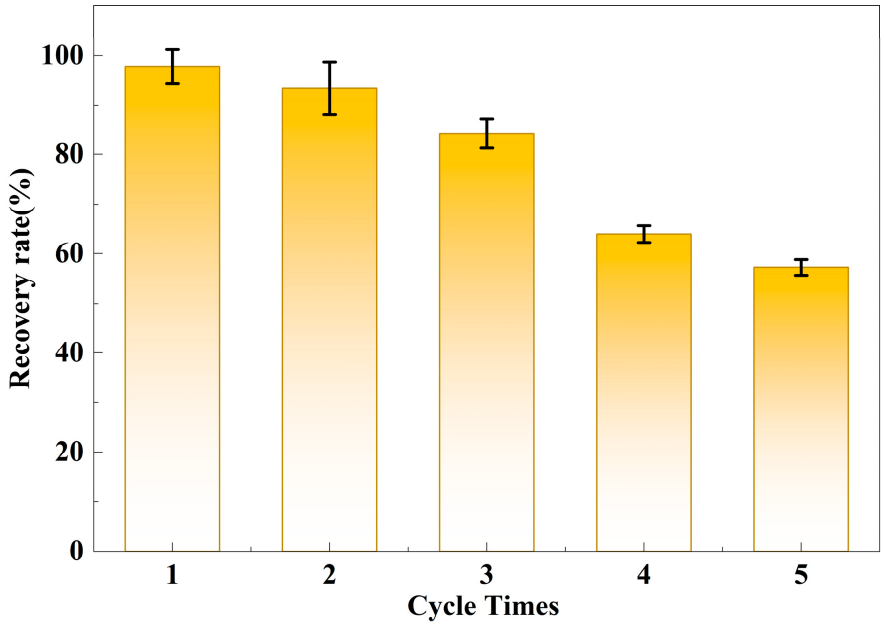

Figure 11. Cyclic recovery efficiency.

During the five adsorption cycles, the gold ion concentrations in the supernatant were 0.45, 1.33, 3.16, 7.21, and 8.55 mg/L, respectively, corresponding to a gold recovery efficiency of 57.25% after five cycles. The results indicate that the recovery efficiency of the modified carbon gradually decreased with increasing cycle number. This is attributed to the presence of Fe^{3+} ions in the eluent, which, under acidic conditions, damage the C=S bonds of the grafted thiourea molecules, leading to a gradual decline in adsorption capacity [33]. After three cycles, the thiourea-modified carbon maintained a recovery rate of 84.2%, demonstrating good reusability.

3.2.7. Comparison of Adsorption Capacity Before and After Modification

To evaluate the enhancement of gold adsorption performance by thiourea grafting, 10 mg each of unmodified commercial activated carbon (AC), oxidized activated carbon (Oxide-AC), and AC-NCS were added to 50 mL of a 30 mg/L chloroauric acid solution. The mixtures were adsorbed at room temperature under stirring at 300 r/min for 1 h. The adsorption capacities were measured and compared, and the results are shown in Figure 12. After oxidation, the adsorption capacity of activated carbon decreased slightly, which is attributed to the increased negative surface charge of the oxidized activated carbon, which hinders the adsorption of $AuCl_4^-$. After modification, the adsorption capacities of activated

carbon were increased by factors of 5.76 and 5.99, respectively, fully demonstrating that this grafting strategy significantly enhances the adsorption capacity of activated carbon toward $AuCl_4^-$.

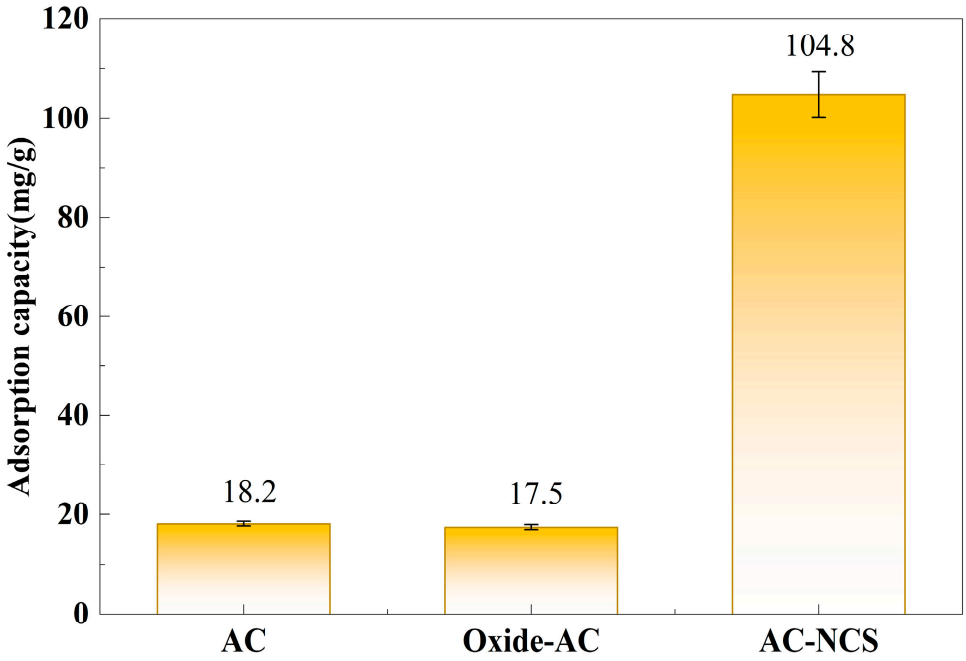

Figure 12. Comparison of adsorption capacity.

3.3. Exploration of Adsorption Mechanism

3.3.1. XPS Photoelectron Spectroscopy Analysis

To elucidate the mechanism of gold ion adsorption and recovery by the adsorbent, the surface chemical states of the samples before and after adsorption were analyzed by XPS, and the results are shown in Figure 13. After adsorption, characteristic Au 4f peaks were detected in the binding energy range of 83–91 eV (Figure 13b). The peak-fitting results indicate that three valence states of gold exist on the surface of the modified carbon after adsorption: Au(0) ($4f_{7/2}$ = 84.0 eV), Au(I) ($4f_{7/2}$ = 85.1 eV), and Au(III) ($4f_{7/2}$ = 86.3 eV), with relative contents of 63.04%, 20.93%, and 16.03%, respectively. SEM observations (Figure S2) further confirm that gold is predominantly present in its elemental state on the adsorbent surface. The predominant presence of Au(0) suggests that reduction is an important driving force in the gold recovery process. The co-existence of Au(I) and Au(III) indicates that a portion of the gold remains on the surface in ionic form and has not been fully reduced.

The N 1s peak-fitting results after adsorption (Figure 13c) show that the binding energy of the amide groups (400.34 eV) did not change significantly, indicating that the nitrogen atoms of the amide bonds do not participate in gold recovery. The binding energy of the protonated amino groups shifted from 402.15 eV before adsorption to 403.18 eV after adsorption, suggesting that the electron cloud density around the nitrogen atoms of the protonated primary amines decreased during adsorption, thereby acting as positive centers to capture $AuCl_4^-$ through electrostatic attraction. In Figure 13d, the binding energy of the sulfur atoms of thiourea increased slightly (by 0.2 eV), which is due to the partial transfer of electrons from sulfur to gold ions, resulting in mild oxidation of sulfur.

The above XPS results indicate that the adsorption mechanism of the modified carbon toward gold is a synergistic "reduction–electrostatic adsorption" effect.

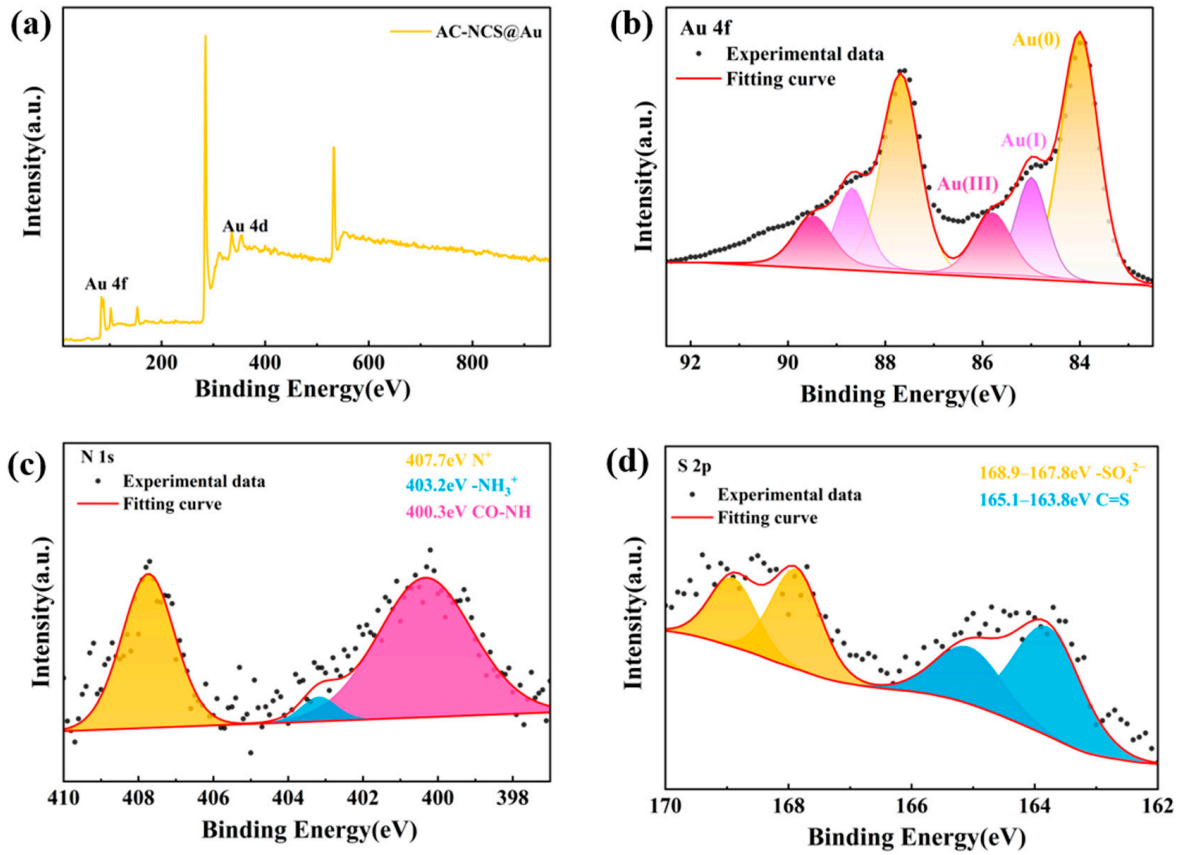

Figure 13. (**a**) XPS survey spectrum after adsorption, (**b**) high-resolution Au 4f, (**c**) N 1s, and (**d**) S 2p spectra.

3.3.2. FT-IR Characterization and Analysis After Adsorption

The changes in functional groups of the modified carbon after $AuCl_4^-$ adsorption under acidic conditions were investigated by FT-IR spectroscopy. The results (Figure 14) show that the bending vibration peak of the primary amine shifted from 1574 cm^{-1} to 1572 cm^{-1}, indicating that no redox reaction occurred during the adsorption process. This is consistent with the conclusion from XPS analysis that the protonated primary amines capture $AuCl_4^-$ via electrostatic attraction. The sulfur-related peak shifted from 1184 cm^{-1} to 1051 cm^{-1}, suggesting that the sulfur atoms were oxidized after adsorption, generating sulfoxide or sulfone species.

Combining the XPS and FT-IR analyses, it can be concluded that there are two types of active sites on the surface of the activated carbon for capturing $AuCl_4^-$. One is the protonated primary amine site, which carries a positive charge under acidic conditions and efficiently captures negatively charged $AuCl_4^-$ through electrostatic interaction. The other is the sulfur-containing site (C=S), which coordinates with $AuCl_4^-$ and gradually reduces $AuCl_4^-$ to elemental gold. The synergistic effect of these two types of sites significantly enhances the adsorption and recovery capacity of activated carbon toward $AuCl_4^-$.

Compared with conventional carbon-based adsorbents (Table 4), the thiourea-grafted modified carbon developed in this work does not require high energy consumption and is well-suited for the recovery of gold ions from low-concentration solutions. Furthermore, this grafting strategy can be readily extended to other carbonaceous substrates with a higher density of anchoring sites, such as graphene oxide and biomass-derived activated carbon, potentially leading to even higher adsorption capacities.

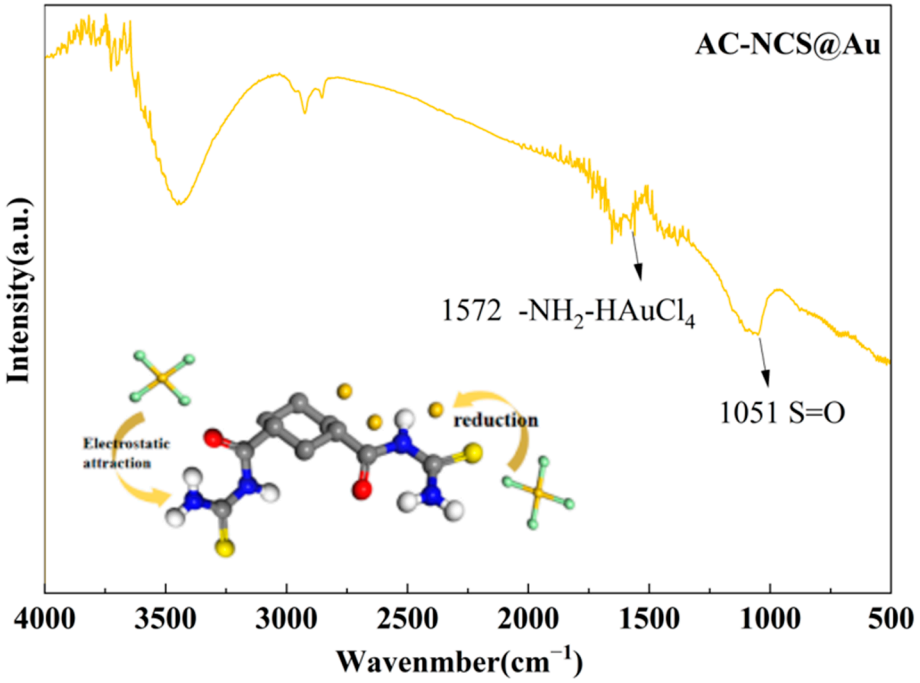

Figure 14. FT-IR spectrum after adsorption.

Table 4. Comparison of Au adsorption capacities of various carbon-based adsorbents reported in the literature and this work.

Carbon-Based Adsorbent	Adsorption Capacity (mg/g)	Reference
Palm-biomass-derived activated carbon	64	[34]
thermal decomposition thiourea-modified carbon (NCS-AC)	12	[19]
Reduced graphene oxide	1606	[35]
Hollow N-doped carbon spheres	305	[36]
Thiourea grafted activated carbon (AC-NCS)	105	This work

4. Conclusions

In this study, a thiourea-grafted activated carbon (AC-NCS) was prepared using a relatively environmentally friendly method. Various characterization techniques confirmed the feasibility of chemically grafting thiourea molecules. The functional groups were designed to enable rapid adsorption and recovery of $AuCl_4^-$ while maintaining a degree of selectivity in complex solutions. The grafting mode is chemical bonding, endowing the material with reusability. The specific findings are as follows:

(1) Raman, FT-IR, and XPS analyses of AC-NCS confirmed that thiourea molecules were successfully grafted onto the activated carbon surface. During the grafting process, the carbon skeleton structure remained stable, with a slight increase in the degree of disorder.

(2) Through the amidation reaction, sulfur- and amino-containing functional groups, which exhibit strong binding affinity toward $AuCl_4^-$, were introduced onto the activated carbon surface. AC-NCS demonstrated a high adsorption capacity (104.76 mg/g) in adsorption experiments, and the adsorption process was dominated by an endothermic chemisorption mechanism. After three cycles of reuse, the

thiourea-modified activated carbon still maintained 84.2% of its initial adsorption capacity, indicating good recyclability.

(3) XPS and FT-IR analyses revealed the adsorption mechanism of AC-NCS toward gold: both sulfur atoms and amino groups participate in the adsorption and reduction of $AuCl_4^-$. The sulfur atoms coordinate with $AuCl_4^-$, and during this process, the electron-donating sulfur atoms transfer electrons to $AuCl_4^-$, reducing the coordinated $AuCl_4^-$ to elemental gold. Additionally, under acidic conditions, the primary amine groups become protonated, acquiring a positive charge and capturing $AuCl_4^-$ via electrostatic attraction. Through this synergistic mechanism of coordination and electrostatic adsorption, efficient and selective adsorption of $AuCl_4^-$ is achieved.

This study validates the feasibility of thiourea grafting via amidation in the NHS/EDC-HCl system. Future efforts may focus on (1) elucidating the effects of surface carboxyl concentration and its interaction with NHS/EDC-HCl to enhance grafting efficiency; and (2) addressing the trade-off between gold desorption efficiency and the stability of the modified carbon, given that the thiourea-Fe^{3+} eluent used herein degrades the grafted thiourea.

Supplementary Materials: The following supporting information can be downloaded at https://www.mdpi.com/article/10.3390/separations13060178/s1: SI-1: Material and Reagents and SI-2: Fitting Models and Formulae. Figure S1: Pseudo-first-order kinetic plot ($\ln(q_e - q_t)$ vs. t). (The scattered points deviate significantly from linearity); Figure S2: Scanning electron microscopy (SEM) image of gold; Table S1: Reagents.

Author Contributions: Conceptualization, T.C. and Y.L.; methodology, T.C. and J.Z.; validation, T.C., J.Z. and Y.L.; formal analysis, T.C., Y.L. and X.L.; investigation, T.C. and J.Z.; resources, X.Z.; data curation, T.C.; writing—original draft preparation, T.C.; writing—review and editing, T.C., X.L. and Y.L.; visualization, T.C.; supervision, X.Z. and X.L.; project administration, X.Z.; funding acquisition, X.Z. All authors have read and agreed to the published version of the manuscript.

Funding: This research was financially supported by the National Natural Science Foundation of China (Nos. 52504443, 22268048 and 52404327).

Data Availability Statement: The original contributions presented in this work are included in the article. The data that support the findings of this study are available on request from the corresponding author.

Conflicts of Interest: The authors declare no conflicts of interest.

References

1. Yang, H.K.; Cao, K.; Han, Y.; Wen, M.; Guo, J.M.; Tan, Z.L.; Lu, J.; Lu, Y. The combined effects of grain and sample sizes on the mechanical properties and fracture modes of gold microwires. *J. Mater. Sci. Technol.* **2019**, *35*, 76–83. [CrossRef]
2. Ning, C.; Lin, C.S.K.; Hui, D.C.W.; McKay, G. Waste Printed Circuit Board (PCB) Recycling Techniques. *Top. Curr. Chem.* **2017**, *375*, 43. [CrossRef] [PubMed]
3. Skandrani, A.; Demers, I.; Kongolo, M. Desulfurization of aged gold-bearing mine tailings. *Miner. Eng.* **2019**, *138*, 195–203. [CrossRef]
4. Dong, N.; Wang, Z.; Wang, J.; Song, W.; Du, L.; Gu, X.; Li, S. Preparation of CPVC-based activated carbon spheres and insight into the adsorption-desorption performance for typical volatile organic compounds. *Environ. Pollut.* **2023**, *343*, 123177. [CrossRef] [PubMed]
5. Geeson, M.B.; Cummins, C.C. Let's Make White Phosphorus Obsolete. *ACS Cent. Sci.* **2020**, *6*, 848–860. [CrossRef] [PubMed]
6. Carlsen, R.; Weckel-Dahman, H.; Swanson, J.M.J. Nernst equilibrium, rectification, and saturation: Insights into ion channel behavior. *Biophys. J.* **2024**, *123*, 4304–4315. [CrossRef] [PubMed]
7. Haflich, H.M.; Coronell, O. Contribution of the transmembrane electric potential to the set voltage in a single-anion exchange membrane electrodialysis-cell and the role of solution conditions. *J. Membr. Sci.* **2025**, *723*, 123925. [CrossRef] [PubMed]
8. Chen, X.; Zhong, Q.-Z.; Qian, Z.; Nguyen, L.B.T.; Chen, J.R.T.; Tan, E.X.; Wang, K.; Song, F.; Richardson, J.J.; Lv, Y.; et al. In situ photo-regenerative phenolic interface for continuous precious metal recovery. *Nat. Water* **2026**, *4*, 360–368. [CrossRef]

9. Ren, J.; Wang, J.; Guo, M.; Li, R.; Guan, Y. Efficient and selective gold recovery from electronic wastewater by synergistic effect between Fe3O4 nanoparticles and quaternary ammonium salt. *J. Environ. Manag.* **2025**, *386*, 125793. [CrossRef] [PubMed]
10. Syed, S. Recovery of gold from secondary sources—A review. *Hydrometallurgy* **2012**, *115*, 30–51. [CrossRef]
11. Rao, M.D.; Singh, K.K.; Morrison, C.A.; Love, J.B. Challenges and opportunities in the recovery of gold from electronic waste. *RSC Adv.* **2020**, *10*, 4300–4309. [CrossRef] [PubMed]
12. Ren, J.; Zhu, Z.; Qiu, Y.; Yu, F.; Zhou, T.; Ma, J.; Zhao, J. Highly selective recovery of gold from strong acidic wastewater with high-purity by self-driven capture. *Chem. Eng. J.* **2023**, *479*, 147585. [CrossRef]
13. Gallagher, N.P.; Hendrix, J.L.; Milosavljevic, E.B.; Nelson, J.H. The Affinity of Carbon for Gold Complexes—Dissolution of Finely Disseminated Gold Using a Flow Electrochemical-Cell. *J. Electrochem. Soc.* **1989**, *136*, 2546–2551. [CrossRef]
14. Aylmore, M.G.; Muir, D.M. Thiosulfate leaching of gold—A review. *Miner. Eng.* **2001**, *14*, 135–174. [CrossRef]
15. Dong, Z.L.; Jiang, T.; Xu, B.; Yang, Y.B.; Li, Q. Recovery of Gold from Pregnant Thiosulfate Solutions by the Resin Adsorption Technique. *Metals* **2017**, *7*, 555. [CrossRef]
16. Sashikesh, G.; Anushkkaran, P.; Praveena, Y.; Arumukham, M.; Kugamoorthy, V.; Kandasamy, V. A comparison study of the efficacy of different activated charcoals derived from Palmyra kernel shell in removing phenolic compounds. *Curr. Res. Green Sustain. Chem.* **2023**, *6*, 100355. [CrossRef]
17. Liang, Q.; Wei, Y.; Hu, L.; Luo, X.; Xiao, X.; Li, H.; Chen, S.; Chen, S.; Ni, C.; Wang, P.; et al. Gold leaching from waste electronic components using ultrasonic-assisted thiourea. *Environ. Technol. Innov.* **2025**, *40*, 104656. [CrossRef]
18. Zheng, J.; Liang, S.; Xiong, Z.; Zhu, J.; Li, Y.; Xiao, C. Study on properties of activated carbon modified by thiourea and adsorption of gold. *Funct. Mater.* **2019**, *50*, 4136–4141+4147.
19. Wang, C.; Chen, S.; Chen, Y.; Zi, F.; Hu, X.; Qin, X.; Zhang, Y.; Yang, P.; He, Y.; He, P.; et al. Modification of activated carbon by chemical vapour deposition through thermal decomposition of thiourea for enhanced adsorption of gold thiosulfate complex. *Sep. Purif. Technol.* **2020**, *241*, 116632. [CrossRef]
20. Fronczak, M.; Pyrzyńska, K.; Bhattarai, A.; Pietrowski, P.; Bystrzejewski, M. Improved adsorption performance of activated carbon covalently functionalised with sulphur-containing ligands in the removal of cadmium from aqueous solutions. *Int. J. Environ. Sci. Technol.* **2019**, *16*, 7921–7932. [CrossRef]
21. de la Torre-Miranda, N.; Reilly, L.; Eloy, P.; Poleunis, C.; Hermans, S. Thiol functionalized activated carbon for gold thiosulfate recovery, an analysis of the interactions between gold and sulfur functions. *Carbon* **2023**, *204*, 254–267. [CrossRef]
22. Figueiredo, J.L.; Pereira, M.F.R.; Freitas, M.M.A.; Órfão, J.J.M. Modification of the surface chemistry of activated carbons. *Carbon* **1999**, *37*, 1379–1389. [CrossRef]
23. Hou, C.X.; Wang, J.; Du, W.; Wang, J.C.; Du, Y.; Liu, C.T.; Zhang, J.X.; Hou, H.; Dang, F.; Zhao, L.L.; et al. One-pot synthesized molybdenum dioxide-molybdenum carbide heterostructures coupled with 3D holey carbon nanosheets for highly efficient and ultrastable cycling lithium-ion storage. *J. Mater. Chem. A* **2019**, *7*, 13460–13472. [CrossRef]
24. e Silva, C.F.L.; Lemões, J.S.; Romani, R.F.; de Oliveira, W.G.; Leite, G.F. Activated Carbon from Residual Lignin Used for Color Removal. *Water Air Soil Pollut.* **2022**, *233*, 177. [CrossRef]
25. Burg, P.; Fydrych, P.; Cagniant, D.; Nanse, G.; Bimer, J.; Jankowska, A. The characterization of nitrogen-enriched activated carbons by IR, XPS and LSER methods. *Carbon* **2002**, *40*, 1521–1531. [CrossRef]
26. Ding, R.; Zhu, Y.; Jing, L.; Chen, S.; Lu, J.; Zhang, X. Sulfhydryl functionalized chitosan-covalent organic framework composites for highly efficient and selective recovery of gold from complex liquids. *Int. J. Biol. Macromol.* **2024**, *282*, 137037. [CrossRef] [PubMed]
27. Li, W.; Yang, J.; Cheng, L.; Gu, Z.; Li, Z.; Li, C.; Hong, Y. KOH/thiourea aqueous solution: A potential solvent for studying the dissolution mechanism and chain conformation of corn starch. *Int. J. Biol. Macromol.* **2022**, *195*, 86–92. [CrossRef] [PubMed]
28. Stöhr, B.; Boehm, H.P.; Schlögl, R. Enhancement of the catalytic activity of activated carbons in oxidation reactions by thermal treatment with ammonia or hydrogen cyanide and observation of a superoxide species as a possible intermediate. *Carbon* **1991**, *29*, 707–720. [CrossRef]
29. Tabet, N.; Faiz, M.; Al-Oteibi, A. XPS study of nitrogen-implanted ZnO thin films obtained by DC-Magnetron reactive plasma. *J. Electron Spectrosc. Relat. Phenom.* **2008**, *163*, 15–18. [CrossRef]
30. Stevens, J.S.; Byard, S.J.; Muryn, C.A.; Schroeder, S.L.M. Identification of Protonation State by XPS, Solid-State NMR, and DFT: Characterization of the Nature of a New Theophylline Complex by Experimental and Computational Methods. *J. Phys. Chem. B* **2010**, *114*, 13961–13969. [CrossRef] [PubMed]
31. Jin, Z.; Pan, J.; Xue, Z.; Li, B.; Yang, L.; Yan, L.; Yin, K.; Shao, P.; Luo, S. Hierarchical recovery of gold and silver from secondary resources using D-cysteine-functionalized activated carbon: High capacity, selectivity, and economic feasibility. *Mater. Today* **2026**, *94*, 103254. [CrossRef]
32. Tiraboschi, G.; Gresh, N.; Giessner-Prettre, C.; Pedersen, L.G.; Deerfield, D.W. Parallelab initio and molecular mechanics investigation of polycoordinated Zn(II) complexes with model hard and soft ligands: Variations of binding energy and of its components with number and charges of ligands. *J. Comput. Chem.* **2000**, *21*, 1011–1039. [CrossRef]

33. Li, J.; Miller, J.D. A Review of Gold Leaching in Acid Thiourea Solutions. *Miner. Process. Extr. Metall. Rev.* **2006**, *27*, 177–214. [CrossRef]
34. Firmansyah, M.L.; Nur Rohman, G.A.; Ullah, N. Machine-Learning-Optimized Palm-Biomass-Derived Activated Carbon Adsorbent for Gold Recovery from Mobile Leachate. *ACS Sustain. Resour. Manag.* **2025**, *2*, 825–832. [CrossRef]
35. Ebrahimi-Moghaddam, S.; Hamidi, A.; Sharifian, S.; Vahidi, E.; Azadmehr, A.; Rashchi, F. Gold adsorption on upcycled reduced graphene oxide in hypochlorite-chloride system: Functionality, mechanism, surface characterization, and environmental impacts. *Sep. Purif. Technol.* **2025**, *382*, 135855. [CrossRef]
36. Fang, C.; Liu, H.; Yin, Z.; Zhu, Z.; Shi, Y.; Meng, W.; Zhu, H.; Li, M. Surface curvature-driven adsorption-reduction mechanism over hollow N-doped carbon enhances recovery of precious metal ions from wastewater. *Environ. Res.* **2025**, *269*, 120914. [CrossRef] [PubMed]